European Journal of Mechanics B/Fluids 28 (2009) 722–727

Contents lists available at ScienceDirect

European Journal of Mechanics B/Fluids

journal homepage: www.elsevier.com/locate/ejmflu

Instability of a slip flow in a curved channel formed by two concentric cylindrical surfaces

A.A. Avramenko [a], A.V. Kuznetsov [b,*]

[a] Institute of Engineering Thermophysics, National Academy of Sciences, Kiev 03057, Ukraine
[b] Dept. of Mechanical and Aerospace Engineering, North Carolina State University, Campus Box 7910, Raleigh, NC 27695-7910, USA

ARTICLE INFO

Article history:
Received 22 August 2008
Received in revised form
1 May 2009
Accepted 11 June 2009
Available online 21 June 2009

Keywords:
Slip flow
Curved microchannel
Linear instability analysis
Taylor number
Dean number

ABSTRACT

Instability of a slip flow in a curved channel formed by two concentric cylindrical surfaces is investigated. Two cases are considered. In the first (Taylor–Couette flow) case the flow is driven by the rotation of the inner cylindrical surface; no azimuthal pressure gradient is applied. In the second case (Dean flow) both cylindrical surfaces are motionless, and the flow is driven by a constant azimuthal pressure gradient. The collocation method is used to find numerically the critical values of the Taylor and Dean numbers, which establish the instability criteria for these two cases. The dependencies of critical values of these numbers on the ratio between the radii of concave and convex walls and on the velocity slip coefficient are investigated.

1. Introduction

Over last few decades, the development of various micro-fluidic devices dictated the increased interest in microchannel flows. These types of flows are found in micro-electro-mechanical systems, bioengineering, as well as in micro-energy systems. In recent years manufacturing processes have been developed to create extremely small machines. Micro-devices refer to systems that have characteristic length on the order of microns. The difficulty of investigating gaseous microscale transport is that scaling laws traditionally used in heat transfer and fluid dynamics do not capture the true behavior of transport in the microscale regime; microscale transport behavior results not so much from rarefaction effects being the result of the reduction in density, but rather from a decrease in the length scales associated with the flow field (Calvert and Baker [1]).

Flows in micro-turbines, micro-compressors, and micro-heat-pumps often occur in curved channels. In this case there are the effects of centrifugal forces. This may lead to centrifugal instability leading to generation of longitudinal vortices. In this paper two cases of centrifugal instabilities in microchannel flows occurring between two concentric cylindrical surfaces are investigated. In the first case (Taylor–Couette flow, Fig. 1a) the inner cylinder is rotating with angular velocity, ω, the outer cylinder is motionless, and there is no azimuthal pressure gradient. In the second case (Dean flow, Fig. 1b) both cylindrical surfaces are motionless, and the flow is driven by a constant azimuthal pressure gradient.

The degree of rarefaction of a gas is determined by the Knudsen number, a parameter defined in this case as the ratio between the mean free path of a gas molecule, L, and the gap between the two cylinders, $R_2 - R_1$ (see Fig. 1a and b). According to Schaaf and Chambre [2], for $\mathrm{Kn} \leq 10^{-2}$ the continuum hypothesis is appropriate and the flow can be analyzed by using the Navier–Stokes equations with conventional no-slip boundary conditions. The range of Knudsen numbers of $10^{-2} \leq \mathrm{Kn} \leq 10^{-1}$ corresponds to the slip flow regime. It should be noted that the boundaries of the slip flow region are somewhat flexible; for example Gad-el-Hak [3] augured that the slip flow occurs in the range of Kundsen numbers of $10^{-3} \leq \mathrm{Kn} \leq 10^{-1}$. For $10^{-1} \leq \mathrm{Kn} \leq 10$ the flow is called the transition flow; the continuum assumption begins to break down and flow is analyzed by such methods as Direct Monte Carlo simulation or using the Burnett equations (Bird [4]).

In the slip flow regime, flows of rarefied gases can be modeled either by using the Boltzmann equation or by Navier–Stokes equations together with a slip boundary condition at the wall. Stefanov and Cercignani [5] and Riechelmann and Nanbu [6] utilized the Boltzmann equation to investigate the Taylor–Couette flow between an inner rotating cylinder and an outer stationary

* Corresponding author. Tel.: +919 515 5292; fax: +919 515 7968.
E-mail address: avkuznet@eos.ncsu.edu (A.V. Kuznetsov).

0997-7546/$ – see front matter © 2009 Elsevier Masson SAS. All rights reserved.
doi:10.1016/j.euromechflu.2009.06.003

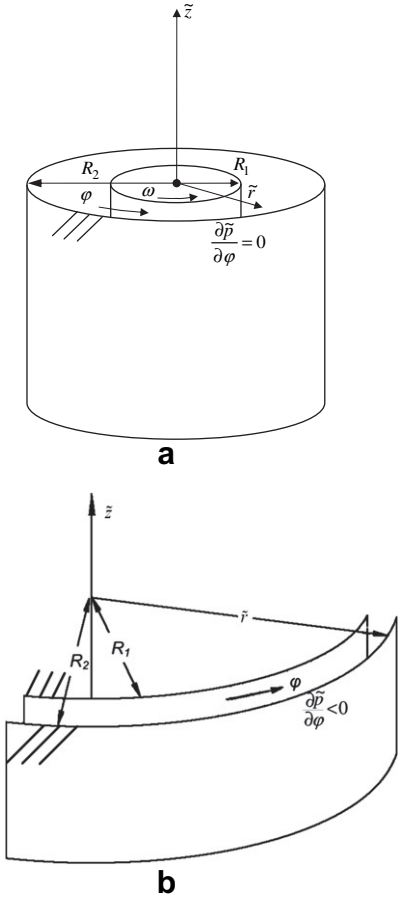

Fig. 1. Schematic diagram: (a) Taylor–Couette flow, (b) Dean flow.

cylinder. Stefanov and Cercignani [5] investigated flow instability and the formation of Taylor vortices for Knudsen numbers of order 10^{-2} and different Mach numbers. In Riechelmann and Nanbu [6] simulations were performed for Knudsen numbers in the range $0.004 < \mathrm{Kn} < 0.04$. The dynamics of formation of Taylor vortices was also investigated. Yoshida and Aoki [7] also investigated the Taylor–Couette slip flow by solving the Boltzmann equation, focusing on the effect of rotation of the outer cylinder on the type of the induced Taylor-vortex flow.

In this paper we adopted the approach based of the utilization of the Navier–Stokes equations combined with a slip boundary condition. We concentrate on obtaining instability criteria for the Taylor–Couette flow as a function of the velocity slip coefficient and the ratio between the radii of concave and convex walls. We also obtain instability criteria for the Dean flow.

For microchannel flows, the slip-flow boundary condition at the wall is modeled by the following equation (Sharipov [8], Cumin et al. [9]):

$$\tilde{u} = \zeta L\left(\frac{\partial \tilde{u}}{\partial \tilde{r}} - \frac{\tilde{u}}{\tilde{r}}\right)\Big|_{\text{wall}}, \tag{1}$$

where $\tilde{r}$ is the radial coordinate, $\tilde{u}$ is the azimuthal velocity component, ζ is the viscous slip coefficient, and L is the mean free path. Modern theory of the viscous slip coefficient can be found in Sharipov and Seleznev [10], Sharipov [11], and Agrawal and Prabhu [12].

Equation (1), in conjunction with Navier–Stokes equations, can be used to model a slip flow in a microchannel. These equations can also be used to model rarified gas dynamics flows typical in vacuum technology (Sharipov [8]).

2. Governing equations and basic flow solution

Flow in the channels, displayed in Fig. 1a and b, is governed by the following equations presented in cylindrical coordinates:

$$\frac{\partial \tilde{w}}{\partial \tilde{t}} + \tilde{v}\frac{\partial \tilde{w}}{\partial \tilde{r}} + \frac{\tilde{u}}{\tilde{r}}\frac{\partial \tilde{w}}{\partial \varphi} + \tilde{w}\frac{\partial \tilde{w}}{\partial \tilde{z}} = -\frac{1}{\rho}\frac{\partial \tilde{p}}{\partial \tilde{z}} + \nu\left(\frac{\partial^2 \tilde{w}}{\partial \tilde{r}^2} + \frac{1}{\tilde{r}}\frac{\partial \tilde{w}}{\partial \tilde{r}} - \frac{\tilde{w}}{\tilde{r}} + \frac{1}{\tilde{r}^2}\frac{\partial^2 \tilde{w}}{\partial \varphi^2} + \frac{\partial^2 \tilde{w}}{\partial \tilde{z}^2}\right) \tag{2}$$

$$\frac{\partial \tilde{v}}{\partial \tilde{t}} + \tilde{v}\frac{\partial \tilde{v}}{\partial \tilde{r}} + \frac{\tilde{u}}{\tilde{r}}\frac{\partial \tilde{v}}{\partial \varphi} - \frac{\tilde{u}^2}{\tilde{r}} + \tilde{w}\frac{\partial \tilde{v}}{\partial \tilde{z}} = -\frac{1}{\rho}\frac{\partial \tilde{p}}{\partial \tilde{r}} + \nu\left(\frac{\partial^2 \tilde{v}}{\partial \tilde{r}^2} + \frac{1}{\tilde{r}}\frac{\partial \tilde{v}}{\partial \tilde{r}} - \frac{\tilde{v}}{\tilde{r}^2} + \frac{1}{\tilde{r}^2}\frac{\partial^2 \tilde{v}}{\partial \varphi^2} - \frac{2}{\tilde{r}^2}\frac{\partial \tilde{u}}{\partial \varphi} + \frac{\partial^2 \tilde{v}}{\partial \tilde{z}^2}\right) \tag{3}$$

$$\frac{\partial \tilde{u}}{\partial \tilde{t}} + \tilde{v}\frac{\partial \tilde{u}}{\partial \tilde{r}} + \frac{\tilde{u}}{\tilde{r}}\frac{\partial \tilde{u}}{\partial \varphi} + \frac{\tilde{u}\tilde{v}}{\tilde{r}} + \tilde{w}\frac{\partial \tilde{u}}{\partial \tilde{z}} = -\frac{1}{\rho\tilde{r}}\frac{\partial \tilde{p}}{\partial \varphi} + \nu\left(\frac{\partial^2 \tilde{u}}{\partial \tilde{r}^2} + \frac{1}{\tilde{r}}\frac{\partial \tilde{u}}{\partial \tilde{r}} - \frac{\tilde{u}}{\tilde{r}^2} + \frac{1}{\tilde{r}^2}\frac{\partial^2 \tilde{u}}{\partial \varphi^2} + \frac{2}{\tilde{r}^2}\frac{\partial \tilde{v}}{\partial \varphi} + \frac{\partial^2 \tilde{u}}{\partial \tilde{z}^2}\right) \tag{4}$$

$$\frac{\partial \tilde{v}}{\partial \tilde{r}} + \frac{\tilde{v}}{\tilde{r}} + \frac{1}{\tilde{r}}\frac{\partial \tilde{u}}{\partial \varphi} + \frac{\partial \tilde{w}}{\partial \tilde{z}} = 0 \tag{5}$$

where $\tilde{r}$, φ, and $\tilde{z}$ are the radial, azimuthal, and axial cylindrical coordinates, respectively; $\tilde{v}$, $\tilde{u}$, and $\tilde{w}$ are the $\tilde{r}$, φ, and $\tilde{z}$ velocity components, respectively; $\tilde{p}$ is the pressure; $\tilde{t}$ is the time; ν is the fluid kinematic viscosity; and ρ is the fluid density.

In order to investigate flow instability the velocity profile of the basic flow is first obtained. This profile is obtained from the azimuthal projection of the momentum equation, equation (4). Since the flow is independent of the azimuthal coordinate φ, all inertia terms are equal to zero. Since the flow is hydrodynamically fully developed, the velocity profile is also independent of the axial coordinate $\tilde{z}$. Then the basic flow is obtained from the azimuthal projection of the momentum equation, which is presented in the following dimensionless form:

$$\frac{d^2u}{d\xi^2} + \frac{1}{\xi}\frac{du}{d\xi} - \frac{u}{\xi^2} = -\frac{1}{\xi}\left(-\frac{\partial p}{\partial \varphi}\right), \tag{6}$$

where dimensionless parameters are defined as:

$$u = \frac{\tilde{u}}{U_m}, \quad p = \frac{\tilde{p}R_2}{U_m\nu\rho}, \quad \xi = \frac{\tilde{r}}{R_2} = \eta + (1-\eta)\left(r + \frac{1}{2}\right),$$
$$\eta = \frac{R_1}{R_2}, \quad r = \frac{\tilde{r} - (R_1 + R_2)/2}{h} \tag{7a}$$

In equation (7a), for the Taylor–Couette flow (Fig. 1a), U_m is defined as the velocity at the inner cylindrical surface:

$$U_m = \omega R_1 \tag{7b}$$

while for the Dean flow (Fig. 1b) U_m is defined as the mean flow velocity:

$$U_m = \frac{1}{h}\int_{R_1}^{R_2} \tilde{u}\,d\tilde{r} \tag{7c}$$

where R_1 and R_2 are the radii of the inner and outer cylindrical surfaces, respectively; and $h = R_2 - R_1$ is the width of the gap between the two cylindrical surfaces.

2.1. Basic flow for the Taylor–Couette flow case

For this flow type (Fig. 1a) the azimuthal pressure gradient is equal to zero. Since the right-hand side of equation (6) vanishes, this equation becomes a homogeneous equation. For this case equation (6) must be solved subject to the following boundary conditions:

$$u = 1 + \sigma\left(\frac{du}{d\xi} - \frac{u}{\eta}\right) \quad \text{at} \quad \xi = \eta, \tag{8a}$$

$$u = -\sigma\left(\frac{\mathrm{d}u}{\mathrm{d}\xi} - u\right) \quad \text{at} \quad \xi = 1, \tag{8b}$$

which are the consequence of the slip-flow condition given by equation (1). In equations (8a) and (8b) $\sigma = \zeta L/R_2$.

Equation (6) is the Stokes equation (this homogeneous equation is also known as Euler equation in mathematics); it is solved by using the following Lie subalgebra:

$$q = \xi\frac{\partial}{\partial\xi} \tag{9}$$

This subalgebra generates the following substitution

$$\xi = \exp(\xi^*) \tag{10}$$

which transforms equation (6) into an equation with constant coefficients. The solution is

$$u = \frac{\eta^2}{r}\,\frac{1 + r^2(2\sigma - 1)}{\eta + 2\sigma + \eta^3(2\sigma - 1)}. \tag{11}$$

For no-slip boundary conditions at the cylindrical walls the velocity distribution given by equation (11) reduces to a well-known velocity distribution obtained in Walowit et al. [13]:

$$u = \frac{\eta}{r}\,\frac{1 - r^2}{1 - \eta^2}. \tag{12}$$

2.2. Basic flow for the Dean flow case

In this case (Fig. 1b), the basic flow is driven by the azimuthal pressure gradient and occurs along the azimuthal coordinate φ. The azimuthal pressure gradient does not depend on the radial position and takes on a constant value. Hence, equation (6) becomes a non-homogeneous ordinary differential equation of the second order. This equation is solved subject to the following boundary conditions:

$$\begin{aligned} u &= \sigma\left(\frac{\mathrm{d}u}{\mathrm{d}\xi} - \frac{u}{\eta}\right) \quad \text{at} \quad \xi = \eta, \\ u &= -\sigma\left(\frac{\mathrm{d}u}{\mathrm{d}\xi} - u\right) \quad \text{at} \quad \xi = 1, \end{aligned} \tag{13}$$

Using substitution (10) and the method of variation of parameters the following solution for the basic flow is obtained:

$$\begin{aligned} u = {} & \big[4(1-\eta)\big[\sigma(1+\eta)\big(r^2(2\sigma(\eta-1)-\eta)^2+\eta^2\big) + r^2\big(2\sigma+\eta \\ & + \eta^3(2\sigma-1)\big)\ln r - \eta^3\big(1 + r^2(2\sigma-1)\big)\ln r\big] \\ & \times \big[r(1+\eta)\big((\eta^2-1)\big(4\sigma^2(\eta-1) - \eta(\eta-1) + 2\sigma(\eta^2+1)\big) \\ & - 4\sigma\eta^2\ln\eta\big)\big]^{-1} \end{aligned} \tag{14}$$

For the case of no-slip boundary conditions at the cylindrical surfaces the velocity distribution given by equation (14) collapses to that obtained by Dean [14]:

$$u = \frac{4(1-\eta)\xi}{4\eta^2\ln^2\eta - (1-\eta^2)^2}\left[(1-\eta^2)\ln\xi + \eta^2\ln\eta\left(1 - \frac{1}{\xi^2}\right)\right] \tag{15}$$

3. Linear instability analysis

Small disturbances to the basic flow are introduced as follows:

$$u = u_0(r) + u_{\mathrm{A}}(r)\cos(\gamma z)\exp[\beta t], \tag{16}$$

$$v = v_{\mathrm{A}}(r)\cos(\gamma z)\exp[\beta t], \tag{17}$$

$$w = w_{\mathrm{A}}(r)\sin(\gamma z)\exp[\beta t], \tag{18}$$

$$p = p_0(r) + p_{\mathrm{A}}(r)\cos(\gamma z)\exp[\beta t], \tag{19}$$

where $u_0(r)$ and $p_0(r)$ are the dimensionless azimuthal velocity and pressure of the basic flow, respectively; u_{A}, v_{A} and w_{A} are the dimensionless amplitudes of disturbance of the azimuthal, radial and axial velocities, respectively; and p_{A} is the dimensionless amplitude of pressure. Additional dimensionless parameters in equations (16)–(19) are defined as follows:

$$\gamma = \tilde{\gamma}h, \quad \beta = \tilde{\beta}h^2/\nu, \quad t = \tilde{t}\nu/h^2, \tag{20}$$

where γ is the wave number, $\tilde{\gamma}$ is the dimensionless wave number, $\tilde{\beta}$ is the amplification factor, β is the dimensionless amplification factor, and t is the dimensionless time.

Since there are no two competing instability mechanisms, the necessary condition for the existence of overstability is not met. Therefore, on physical grounds, instability is monotonic and β is a real number. This is a standard assumption for instability analysis for a flow in a curved channel formed by two concentric cylindrical surfaces, which is utilized in Walowit et al. [13], Dean [14], Reid [15], and Hämmerlin [16]. Walowit et al. [13] also pointed out that experimental results show no evidence of a purely oscillatory motion but rather indicate the existence of a new stationary cellular motion (Taylor or Dean vortices, depending on the type of the flow) thus supporting the monotonic instability assumption.

Substituting equations (16)–(19) into equations (2)–(5), linearizing, eliminating the amplitudes w_{A} and p_{A}, and setting $\beta = 0$, which corresponds to the neutral stability curve, the following equations for the azimuthal and radial amplitudes are obtained:

$$(DD^* - \gamma^2)u_{\mathrm{A}} = D^*Uv_{\mathrm{AR}}, \tag{21}$$

$$(DD^* - \gamma^2)^2 v_{\mathrm{AR}} = 2\gamma^2 AUu_{\mathrm{A}}, \tag{22}$$

where

$$D = \frac{d}{dr}, \quad D^* = D + \frac{1-\eta}{\xi}, \tag{23}$$

$$\nu_{AR} = \mathrm{Re}\,\nu_A, \tag{24}$$

$$A = \mathrm{Ta}^2\eta \tag{25}$$

for the Taylor–Couette flow and

$$A = \mathrm{De}^2 \tag{26}$$

for the Dean flow. Here

$$\mathrm{Ta} = \frac{U_m h}{\nu}\sqrt{\frac{h}{R_1}}, \quad \mathrm{De} = \frac{U_m h}{\nu}\sqrt{\frac{h}{R_2}}, \quad \mathrm{Re} = \frac{U_m h}{\nu}, \tag{27}$$

are the Taylor, Dean, and Reynolds numbers, respectively.

The criterion of hydrodynamic instability that leads to the development of secondary vortices is obtained by solving the eigenvalue problem for equations (21) and (22) subject to boundary conditions given by equation (1) at both cylindrical walls. The result of the solution of the eigenvalue problem is the following dependence:

$$\mathrm{Ta} = \mathrm{Ta}(\gamma, \eta, \sigma) \tag{28}$$

for the Taylor–Couette flow and

$$\mathrm{De} = \mathrm{De}(\gamma, \eta, \sigma) \tag{29}$$

for the Dean flow.

The instability criterion is then given by the following equation:

$$\mathrm{Ta}_{cr} = \min_{\gamma}\{\mathrm{Ta}(\gamma, \eta, \sigma)\} \tag{30}$$

for the Taylor–Couette flow and

$$\mathrm{De}_{cr} = \min_{\gamma}\{\mathrm{De}(\gamma, \eta, \sigma)\} \tag{31}$$

for the Dean flow. In equations (30) and (31) the minimum is taken with respect to γ, the values of η and σ are kept constant calculating the minimum.

4. Numerical solution and analysis

The eigenvalue problem for equations (21) and (22) is solved by the collocation method (Fletcher [17]). First, test computations are carried out to validate the numerical code as well as the choice

Table 1
Comparison of present results for $\sigma = 0$ with data presented in Walowit et al. [13] and Reid [15].

η	This paper		Data of Walowit et al. [13]		Reid [15]	This paper		Data of Walowit et al. [4]	
	γ_{cr}	De_{cr}	γ_{cr}	De_{cr}	De_{cr}	γ_{cr}	Ta_{cr}	γ_{cr}	Ta_{cr}
1	3.96	35.93	3.96	37.31	35.94	3.127	41.18858	3.12	41.18
0.95	4.0	36.35	4.02	37.7		3.127	42.43466	3.12	42.45
0.9	4.04	36.85	4.06	38.3		3.13	43.8724	3.13	43.88
0.8	4.11	37.98	4.16	39.51					
0.7	4.19	39.4	4.24	40.96		3.141	52.038	3.14	52.04
0.6	4.27	41.24	4.32	42.73					
0.5	4.4	43.71	4.41	44.91		3.162	68.18627	3.16	68.18
0.4	4.49	47.24	4.46	47.7					
0.3	4.61	52.62	4.51	51.47		3.217	111.8504	3.2	111.889
0.2	4.79	62.28	4.57	57.00					
0.1	4.96	84.42	4.64	65.91		3.346	421.4778	3.3	422.79

Table 2
Effect of parameters η and σ on the critical value of the Taylor number and also on the critical wave number for the flow displayed in Fig. 1a.

η	$\sigma = 0$		$\sigma = 0.1$		$\sigma = 0.2$		$\sigma = 0.3$		$\sigma = 0.4$	
	γ_{cr}	Ta_{cr}	γ_{cr}	Ta_{cr}	γ_{cr}	Ta_{cr}	γ_{cr}	Ta_{cr}	γ_{cr}	Ta_{cr}
0.999	3.12	41.188	4.23	989.2	4.26	1930.1	4.46	2910.7	4.58	3980.1
0.95	3.12	42.43	3.25	115.7	3.34	140.3	3.65	213.5	3.78	289.4
0.9	3.13	43.87	3.18	95.4	3.21	101.0	3.43	123.1	3.63	142.7
0.85	3.13	45.5	3.12	83.4	3.19	97.5	3.30	101.6	3.41	112.5
0.7	3.14	52.03	3.13	78.3	3.23	88.2	3.54	94.7	3.67	107.3
0.5	3.16	68.18	3.16	97.6	3.37	111.4	3.66	120.7	3.79	139.7
0.3	3.21	111.85	3.19	187.8	3.45	243.4	3.78	295.5	3.94	363.6
0.1	3.34	421.47	3.37	1034.4	3.54	1245.0	3.82	1367.4	4.08	1716.8

η	$\sigma = 0.5$		$\sigma = 0.6$		$\sigma = 0.7$		$\sigma = 0.8$		$\sigma = 0.9$	
	γ_{cr}	Ta_{cr}	γ_{cr}	Ta_{cr}	γ_{cr}	Ta_{cr}	γ_{cr}	Ta_{cr}	γ_{cr}	Ta_{cr}
0.999	4.67	5186.5	4.79	6578.0	4.94	8202.7	5.13	10 109	5.67	12 345
0.95	3.98	368.9	4.09	416.1	4.15	978.3	4.68	1901.4	5.46	3267.1
0.9	3.76	175.6	3.95	231.6	4.03	432.1	4/56	757.3	5.11	1235.0
0.85	3.53	144.6	3.67	213.3	3.88	332.6	4.04	518.7	4.87	789.2
0.7	3.89	120.1	3.99	178.2	4.07	281.4	4.16	443.7	4.92	678.9
0.5	3.98	180.5	4.12	256.7	4.26	378.7	4.38	561.4	5.01	817.3
0.3	4.05	464.9	4.25	617.4	4.34	840.6	4.47	1150.8	5.12	1567.2
0.1	4.18	2608.1	4.37	4356.4	4.49	7275.6	4.60	11 682.0	5.28	17 890

Table 3
Effect of parameters η and σ on the critical value of the Dean number and also on the critical wave number for the flow displayed in Fig. 1b.

η	$\sigma=0$		$\sigma=0.1$		$\sigma=0.2$		$\sigma=0.3$		$\sigma=0.4$		$\sigma=0.5$		$\sigma=0.6$		$\sigma=0.7$		$\sigma=0.8$		$\sigma=0.9$	
	γ_{cr}	De_{cr}	γ_{cr}	De_{cr}	γ_{cr}	De_{cr}	γ_{cr}	De_{cr}	γ_{cr}	De_{cr}	γ_{cr}	De_{cr}	γ_{cr}	De_{cr}	γ_{cr}	De_{cr}	γ_{cr}	De_{cr}	γ_{cr}	De_{cr}
0.999	3.95	35.93	3.42	134.2	3.23	143.4	3.11	158.7	2.97	187.5	2.87	209.1	2.75	224.7	2.67	228.5	2.53	231.9	2.34	234.8
0.95	3.98	36.366	3.54	115.7	3.39	126.8	3.25	140.4	3.05	165.7	2.94	184.4	2.82	198.7	2.7	207.9	2.61	209.5	2.47	211.6
0.9	4.02	36.85	3.61	97.4	3.44	112.5	3.32	130.4	3.21	145.4	3.13	151.4	3.07	159.8	2.94	167.6	2.85	174.8	2.69	193.2
0.85	4.06	37.388	3.73	88.3	3.58	106.9	3.45	117.3	3.33	135.9	3.28	141.6	3.12	149.5	3.04	152.1	2.97	165.5	2.76	183.7
0.8	4.1	37.985	3.82	83.3	3.71	98.6	3.62	110.6	3.55	131.7	3.48	133.5	3.34	136.7	3.22	142.0	3.11	159.4	2.97	174.9
0.7	4.18	39.4	3.93	76.4	3.88	92.1	3.74	100.3	3.66	123.1	3.57	127.2	3.43	130.8	3.32	136.6	3.26	147.7	3.08	167.1
0.6	4.28	41.24	4.03	73.1	3.97	82.4	3.85	94.9	3.74	118.3	3.68	123.7	3.52	128.6	3.42	135.1	3.31	145.4	3.19	162.3
0.5	4.39	43.717	4.14	72.5	4.05	79.3	3.98	92.8	3.83	117.0	3.76	119.5	3.63	123.9	3.54	133.6	3.45	143.5	3.29	159.5
0.4	4.49	47.24	4.23	74.1	4.14	86.7	4.04	94.7	3.97	122.2	3.85	125.6	3.74	130.8	3.61	144.6	3.57	151.9	3.32	161.4
0.3	4.65	52.67	4.36	77.6	4.22	91.2	4.15	97.2	4.03	128.6	3.98	132.3	3.83	139.2	3.78	148.9	3.69	155.4	3.48	166.0
0.2	4.79	62.28	4.49	86.0	4.37	106.2	4.24	123.1	4.16	137.8	4.07	148.1	3.96	156.8	3.87	163.5	3.74	168.4	3.57	172.7

of the trial functions. Test computations are performed for $\sigma=0$, which corresponds to no-slip boundary conditions:

$$u_A = v_{AR} = Du_A = 0 \quad \text{at} \quad r = \pm\frac{1}{2}. \tag{32}$$

To estimate the numerical inaccuracy of the method, two different sets of the trial functions are utilized. The first set of the trial functions is:

$$u_A = \sum_{j=1}^{N} a_j\left(r^2-\frac{1}{4}\right)r^{j-1}, \quad v_{AR} = \sum_{j=1}^{N} b_j\left(r^2-\frac{1}{4}\right)^2 r^{j-1}. \tag{33}$$

The second set of the trial functions is:

$$u_A = \sum_{j=1}^{N} a_j\left(r^2-\frac{1}{4}\right)T_{2j-1}(r), \quad v_{AR} = \sum_{j=1}^{N} b_j\left(r^2-\frac{1}{4}\right)^2 T_{2j-1}(r). \tag{34}$$

where $T_j(r)$ are the Chebyshev polynomials of the first kind.

In the case when the Chebyshev polynomials are utilized to construct the trial functions, the orthogonal collocation method is used. In this method, the residuals are calculated at the points where the Chebyshev polynomials are equal to zero. This approach leads to minimization of the maximum inaccuracy (Fletcher [17]).

The test calculations show that for $N=500$, the difference in Ta_{cr} and De_{cr} resulting from using different sets of trial functions (given by Eq. (33) and Eq. (34), respectively) is less than 0.5%. The present data are compared with data of Walowit et al. [13] in Table 1. This table gives critical values of the Taylor and Dean numbers and corresponding wavenumbers. There is a good agreement between the present computational results and the data of Walowit et al. [13] and Reid [15]; Table 1 shows that the discrepancy with the results of Walowit et al. [13] does not exceed 8%, except for $\eta=0.1$. The same value of $De_{cr}=35.94$ for the case $\eta=1$ (if the thickness of the gap, R_2-R_1, is fixed, this corresponds to the limit when both radii are very large, so that the curvature is very small) is obtained in Dean [14] and Hämmerlin [16]. The discrepancy between the present computational results and the results of Walowit's et al. [13] is explained by the small number of terms in the representation of the trial functions in the Galerkin method ($N=4$) used in Walowit et al. [13]; this paper uses $N=500$. The study of sensitivity of the critical Dean number to the number of terms in the representation of the trial functions shows that predictions of De_{cr} improve up to $N=30$; $N=500$ should give a nearly exact solution; $N=4$ used in Walowit et al. [13] is sufficient only for a fairly approximate result.

In order to compute the criteria of centrifugal instability for a slip-flow case the following sets of trial functions are utilized:

$$u_A = \sum_{j=1}^{N} a_j\left(r^2-\frac{1}{4}\right)^2 r^{j-1}, \quad v_{AR} = \sum_{j=1}^{N} b_j\left(r^2-\frac{1}{4}\right)^3 r^{j-1} \tag{35}$$

or

$$u_A = \sum_{j=1}^{N} a_j\left(r^2-\frac{1}{4}\right)^2 T_{2j-1}(r), \quad v_{AR} = \sum_{j=1}^{N} b_j\left(r^2-\frac{1}{4}\right)^3 T_{2j-1}(r) \tag{36}$$

The results obtained using both sets of trial functions are identical. Numerical results are given in Tables 2 and 3; the most characteristic results are also shown in Fig 2a,b.

Tables 2 and 3 show the influence of parameters η and σ on the critical values of the Taylor and Dean numbers and also on the critical wave numbers. As follows from Tables 2 and 3, increasing σ (which is the same as increasing Kn) leads to the increase of the critical values of the Taylor and Dean numbers; this effect is also visible in Fig. 2a,b. This occurs because when σ is increased, the profile of the basic flow becomes more flat. This effect is similar to the effect of the basic flow velocity profile on the instability described by the Orr–Sommerfeld equation. A similar instability for a flow near on a concave wall is investigated in Kobayashi [18]. The effect of σ is also in agreement with findings of Lauga and Cossu [19] who studied turbulence transition for the slip flow in a parallel-plate channel. They established that the value of the critical Reynolds number increases as the value of σ increases. This means that the flow becomes more stable when σ increases. Although the Taylor and Dean instabilities studied in this paper are not related to turbulence transition but rather related to the development of longitudinal vortices, there are certain similarities in the effect of the shape of the velocity profile on the onset of these instabilities. A similar effect for a parallel-plate channel occupied by a hyper-porous medium is found in Avramenko et al. [20]. It should be noted that for values of parameter σ larger or equal to 0.3 the Knudsen number is at a borderline between the slip and transition flow regimes; therefore, the accuracy of the analysis based on the Navier–Stokes equations will somewhat deteriorate as σ is increased beyond 0.3. For these situations, further analysis based on Direct Monte Carlo simulation or using the Burnett equations may be needed.

As one can see from Fig. 2a,b, the dependence of critical Taylor and Dean numbers on η when $\sigma>0$ exhibits a minimum. The critical Taylor number takes on its minimum value at approximately $\eta=0.7$ and the critical Dean number takes on its minimum value at approximately $\eta=0.5$. For the case of no-slip boundary

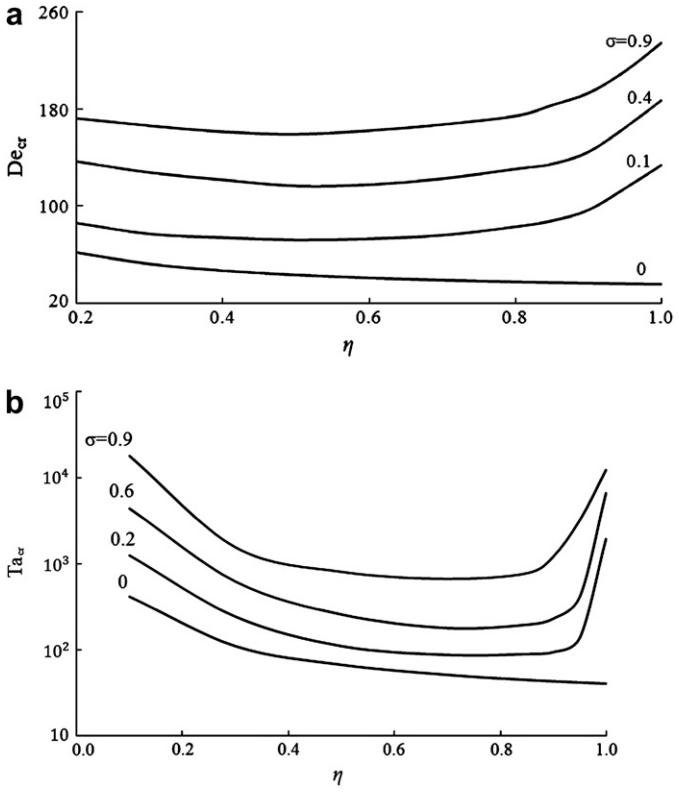

Fig. 2. Critical values of the Dean (a) and Taylor (b) numbers versus parameter η for various values of parameter σ.

conditions ($\sigma = 0$) this minimum is not observed. The existence of the minimum is explained as follows. The increase of parameter η can be interpreted as decreasing the width of the curvilinear channel ($\eta = 1 - h/R_2$, where h is the channel width) and as $\eta \to 1$ the channel becomes a microchannel. When the channel becomes a microchannel, it becomes more difficult for the hydrodynamic instability to develop, which explains why the system becomes more stable as $\eta \to 1$ and the critical values of both Dean and Taylor numbers increase, as shown in Fig. 2a,b. Interestingly, the increase of Ta_{cr} and De_{cr} as $\eta \to 1$ is observed only for $\sigma > 0$ (for the case of slip boundary conditions at the channel walls), that is for the case when the channel behaves as a real microchannel. As $\eta \to 0$ the critical values of both Dean and Taylor numbers also increase, which occurs for any value of σ (for both slip and no-slip boundary conditions at the walls). To explain this, consider, for example, the dependence of Ta_{cr} on η displayed in Fig. 2b. The value of Ta_{cr} can be related to the value of the critical Reynolds number as follows:

$$Ta_{cr}(\eta) = Re_{cr}\sqrt{\frac{1-\eta}{\eta}} \tag{37}$$

As $\eta \to 0$ the value of Re_{cr} remains finite but $1/\eta \to \infty$, which explains the increase of Ta_{cr} as $\eta \to 0$. The increase of De_{cr} as $\eta \to 0$ is explained similarly. Since both Ta_{cr} and De_{cr} increase as $\eta \to 0$ and as $\eta \to 1$, there must be minimums on the curves displaying the dependence of Ta_{cr} and De_{cr} on η; this is exactly what is observed in Fig. 2a,b.

5. Conclusions

Two types of hydrodynamic instabilities of a slip flow in a curved microchannel are investigated, namely, the instability of a slip flow between two concentric cylinders one of which is rotating (Taylor–Couette flow) and the instability of a slip flow between two fixed cylinders driven by a constant azimuthal pressure gradient (Dean flow). The basic velocity profiles for both slip-flow cases are obtained. The linear instability problem is solved numerically by using the collocation method where the trial functions also satisfy the slip-flow conditions at the channel walls. The slip-flow boundary conditions lead to the increase of the fullness of velocity profile of the basic flow (the profile becomes more flat). This, in turn, leads to the increase of the critical values of Taylor and Dean numbers characterizing the onset of hydrodynamic instability in these two cases. It is also shown that for $\sigma > 0$ the dependencies of critical Taylor and Dean numbers on parameter η exhibit a minimum. For the Taylor–Couette flow this minimum occurs at approximately $\eta = 0.7$ and for the Dean flow the minimum occurs at approximately $\eta = 0.5$.

Acknowledgement

The authors gratefully acknowledge NATO Collaborative Linkage Grant (CBP.NUKR.CLG 981714). The authors are grateful to reviewers for their constructive comments and suggestions.

References

[1] M. Calvert, J. Baker, Thermal conductivity and gaseous microscale transport, J. Thermophys. Heat Transf. 12 (1998) 138–145.
[2] S.A. Schaaf, P.L. Chambre, Flow of Rarefied Gases, Princeton University Press, Princeton, 1961.
[3] M. Gad-el-Hak, The fluid mechanics of microdevices – the freeman scholar lecture, ASME J. Fluid. Eng. 121 (1999) 5–33.
[4] G.A. Bird, Molecular Gas Dynamics and the Direct Simulation of Gas Flows, Oxford University Press, Oxford, 1994.
[5] S. Stefanov, C. Cercignani, Monte Carlo simulation of the Taylor–Couette flow of a rarefied gas, J. Fluid Mech. 256 (1993) 199–213.
[6] D. Riechelmann, K. Nanbu, Monte Carlo direct simulation of the Taylor instability in rarefied gas, Phys. Fluid. A 5 (1993) 2585–2587.
[7] H. Yoshida, K. Aoki, A numerical study of Taylor–Couette problem for a rarefied gas: effect of rotation of the outer cylinder, rarefied gas dynamics: 24th international symposium, in: M. Capitelli (Ed.), American Institute of Physics (2005), pp. 467–472.
[8] F. Sharipov, Elements of rarified gas dynamics and numerical approximations, in: Karl Jousten (Ed.), Handbook of Vacuum Technology, Chapter V, Wiley-VCH, Berlin, 2008.
[9] L.M.G. Cumin, G.M. Kremer, F. Sharipov, The influence of slip and jump boundary conditions on the cylindrical Couette flow, Math. Model. Meth. Appl. Sci. 12 (2002) 445–459.
[10] F. Sharipov, V. Seleznev, Data on internal rarefied gas flows, J. Phys. Chem. Ref. Data 27 (1998) 657–706.
[11] F. Sharipov, Application of the Cercignani-Lampis scattering kernel to calculations of rarefied gas flows, Eur. J. Mech. B Fluid. 22 (2003) 133–143.
[12] A. Agrawal, S.V. Prabhu, Deduction of slip coefficient in slip and transition regimes from existing cylindrical Couette flow data, Exp. Therm. Fluid Sci. 32 (2008) 991–996.
[13] J. Walowit, S. Tsao, R.C. DiPrima, Stability of flow between arbitrary spaced concentric cylindrical surfaces including the effect of a radial temperature, ASME J. Appl. Mech. 31 (1964) 585–594.
[14] W.R. Dean, Fluid motion in a curved channel, Proc. R. Soc. A 122 (1928) 402–420.
[15] W.H. Reid, On the stability of viscous flow in a curved channel, Proc. R. Soc. A 244 (1958) 186–198.
[16] G. Hämmerlin, Die Stabilität der Strömung in einem gekrümmten Kanal, Arch. Rational Mech. Anal. 1 (1958) 212–224.
[17] C.A.J. Fletcher, Computational Galerkin Method, Springer-Verlag, New York, 1984.
[18] R. Kobayashi, Stability of laminar boundary layer on a concave permeable wall with homogeneous suction, Report Inst. High Speed Mech 27 (1973) 31–47.
[19] E. Lauga, C. Cossu, A note on the stability of slip channel flows, Phys. Fluids 17 (2005) article 088106.
[20] A.A. Avramenko, A.V. Kuznetsov, D.A. Nield, Instability of slip-flow in a channel occupied by a hyper-porous medium, J. Porous Media 10 (2007) 435–442.